# Constitutive Relations for Macroscopic Modelling of Equiaxed Solidification

**M. Torabi Rad[1], M. Založnik[2], H. Combeau[2], and C. Beckermann[1]**

[1] Department of Mechanical and Industrial Engineering, University of Iowa, Iowa City, IA 52242, USA
[2] Institut Jean Lamour, CNRS – Université de Lorraine, F-54011 Nancy, France

## Abstract

Macroscopic models of equiaxed solidification in an undercooled melt consist of conservation and constitutive relations. Currently available constitutive relations assume highly simplified envelope shapes and diffusion conditions and have not been validated. Simulation results from a previously developed mesoscopic envelope model are used to develop more realistic constitutive relations for envelope sphericity, primary tip and volume-equivalent sphere velocities, and average diffusion length. These relations are verified against the mesoscopic results and can now be used, in macroscopic models of equiaxed solidification, to incorporate more realistically the average growth kinetics and solute diffusion rates.

*Keywords: Macroscopic Modelling, Mesoscopic Model, Equiaxed Solidification.*

## 1. Introduction

In macroscopic models of equiaxed solidification in an undercooled melt, the average growth kinetics of and solute diffusion rates from the dendrite envelopes inside a representative elementary volume (REV), are described by the conservation equations [1, 2]:

$$\frac{dg_\epsilon}{dt} = -S_{env} w_{env} \tag{1}$$

$$\frac{\partial}{\partial t}\left(g_\epsilon \overline{C}_\epsilon\right) = \frac{\partial g_\epsilon}{\partial t} C_l^* + S_{env} \frac{D_l}{\delta_{env}}\left(C_l^* - \overline{C}_\epsilon\right) \tag{2}$$

where $g_\epsilon$, $S_{env}$, $w_{env}$, $\overline{C}_\epsilon$, $C_l^*$, $D_l$, and $\delta_{env}$ are the extradendritic liquid fraction, envelope surface area per unit volume of the REV, average envelope growth velocity, average solute concentration in the extradendritic liquid, equilibrium solute concentration in the liquid, solute mass diffusivity in the liquid, and average diffusion length around the envelopes, respectively. The variables $S_{env}$, $w_{env}$, and $\delta_{env}$ need to be obtained from constitutive relations. Currently available constitutive relations assume highly simplified envelope shapes and diffusion conditions and have not been validated. In the present study, simulation results from the mesoscopic envelope model of Souhar et al. [3] are used to develop more realistic constitutive relations for equiaxed dendritic growth in an undercooled melt.

## 2. Mesoscopic simulations

The reader is referred to Souhar et al. [3] for the details of the mesoscopic model. In the mesoscopic simulations, the evolution of the dendrite envelopes and solute diffusion field in the extradendritic liquid are resolved directly on a spatial scale that corresponds to a REV. Simulations were performed for isothermal growth of a single grain growing into an essentially infinite domain (Figure 1a) and for multiple grains (Figure 1b) with high/low grain densities of $R_f/(D_l/V_{Iv}) = 4.03/6.31$, where $R_f$ and $V_{Iv}$ are the final grain radius and Ivantsov tip velocity at the initial undercooling $\Omega_0$, respectively. For the multigrain cases, the grains were arranged periodically in a BCC lattice, with the primary arms growing along the axes (Figure 1b). Each case was simulated for $\Omega_0 = 0.05$ and 0.15. Results were first averaged over the REV (upscaled), to obtain time evolutions of $g_\epsilon$, $\overline{C}_\epsilon$, $S_{env}$, $w_{env}$, and $\delta_{env}$, and then the upscaled results were used to develop constitutive relations for $S_{env}$, $w_{env}$, and $\delta_{env}$.

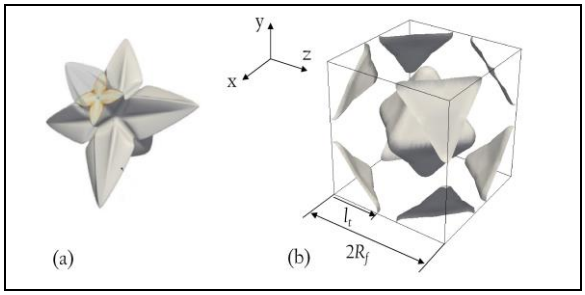


**Figure 1:** Mesoscopic grain envelopes for (a) a single grain and (b) multiple grains in a BCC arrangement with the primary arms growing along the x, y, and z axes.

# 3. Governing equations

The envelope variables $S_{env}$, $w_{env}$, and $\delta_{env}$ are first related to volume-equivalent sphere variables $S_{sp}$, $w_{sp}$, and $\delta_{sp}$ through the envelope sphericity $\psi$ as:

$$w_{env} = \psi w_{sp}; \quad S_{env} = \frac{S_{sp}}{\psi}; \quad \frac{\delta_{env}}{\delta_{sp}} = \frac{\delta_{env}}{\delta_{sp}}(\psi) \tag{3}$$

The evolution of the sphericity of the dendrite envelopes is also obtained from the mesoscopic simulation results. Sphere variables are then calculated from

$$\frac{w_{sp}}{V_t} = \frac{w_{sp}}{V_t}(\psi); \quad S_{sp} = \frac{3(1-g_e)}{R_{sp}}; \quad \frac{dR_{sp}}{dt} = w_{sp}; \quad \delta_{sp}^{FG} = R_{sp}\left[1 - Iv(\mathrm{Pe}_{sp})\right] \tag{4}$$

where $V_t$ is the primary dendrite tip velocity, $\mathrm{Pe}_{sp} \equiv w_{sp}R_{sp}/D_l$ and $R_{sp}$ are the sphere growth Péclet number and radius, respectively, and $\delta_{sp}^{FG}$ is the free-growth diffusion length. The fourth equality is the free-growth limit ($R_f \to \infty$) of the relation developed by Martorano et al. [3], which, due to the space limitations, is not provided here. The last equality in Equation 3 and the first equality in Equation 4 indicate that $\delta_{env}/\delta_{sp}$ and $w_{sp}/V_t$ are assumed to be functions of $\psi$ only. The sphericity $\psi$ itself is assumed to be a function of $l_t/l_{diff}$ only, where $l_t$ is the primary arm length, calculated from $dl_t/dt = V_t$, and $l_{diff} = D_l/V_t$ is the instantaneous diffusion length ahead of the tip, i.e.:

$$\psi = \psi(l_t/l_{diff}) \tag{5}$$

The dendrite tip velocity $V_t$ is calculated from the stagnant film formulation of the Ivantsov solution [4]:

$$\Omega_e = Pe_t \exp(Pe_t)\left\{\mathrm{E}_1(Pe_t) - \mathrm{E}_1\left[Pe_t\left(1 + 2\delta_f/R_t\right)\right]\right\} \tag{6}$$

where $\Omega_e = \left(C_l^* - \bar{C}_e\right)/\left[(1-k_0)C_l^*\right]$ is the average undercooling in the extradendritic liquid, $\mathrm{Pe}_t = V_t R_t/(2D_l)$ is the dendrite tip Péclet number, $R_t = \sqrt{d_0 D_l/(V_t\sigma^*)}$ is the tip radius, $k_0$ is the partition coefficient, $d_0$ is the capillary length, and $\sigma^*$ is the tip selection parameter. The stagnant film thickness $\delta_f$, scaled by $l_{diff}$, is assumed to be a function of the scaled length of the liquid region ahead of the tip up to the symmetry line between two adjacent grains, $l_l^*$:

$$\frac{\delta_f}{l_{diff}} = \frac{\delta_f}{l_{diff}}(l_l^*); \quad l_l^* = \frac{R_f - l_t}{l_{diff}} \tag{7}$$

# 4. Results and discussion

In the following figures, mesoscopic results for a single grain are shown as black curves and for multiple grains with high/low grain density as red/blue curves. Results for $\Omega_0 =$ 0.05 and 0.15 are plotted as solid and dashed curves, respectively. Purple curves depict our curve fits, and thick and thin curves represent predicted (from our fits) and mesoscopic results, respectively.

In Figure 2, the sphericity $\psi$ is plotted as a function of the scaled primary dendrite arm length, $l_t/l_{diff}$. It can be seen that for a single grain, the mesoscopic simulation results for the two different initial undercoolings $\Omega_0$ collapse onto a single curve. This indicates that the sphericity is indeed a function of $l_t/l_{diff}$ only. The multigrain data in the plot fall on the same curve as the single grain data as long as $l_t/l_{diff}$ is increasing. However, when $l_t/l_{diff}$ starts decreasing, which occurs because $V_t$ in the expression for $l_{diff}$ decreases due to solutal interactions between grains, the multigrain data start to deviate from the sphericity curve for a single grain. The variation of $\psi$ when $l_t/l_{diff}$ is decreasing are, however, relatively small and are neglected here. The final fit of the sphericity data for both the single grain and the multigrain cases can, is then given by:

$$d(l_t/l_{diff}) > 0 \to \psi = 0.31 + 0.69\exp\left\{-0.12\left[(l_t - R_0)/l_{diff}\right]\right\}$$
$$d(l_t/l_{diff}) < 0 \to d\psi = 0 \tag{8}$$

where $R_0 = 0.85 D_l/V_{Iv}$ is the radius of the initial spherical seed in the mesoscopic simulations.

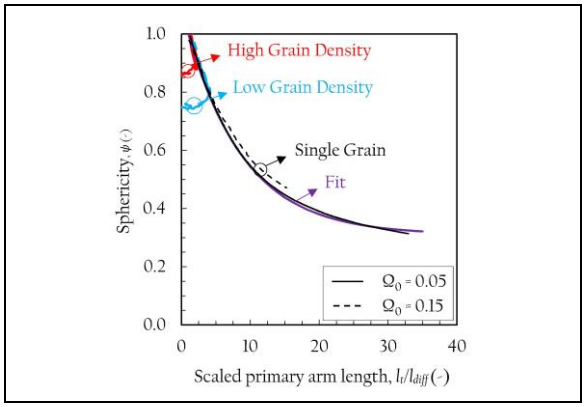


**Figure 2:** Envelope sphericity, $\psi$, as a function of the scaled primary dendrite arm length, $l_t/l_{diff}$.

In Figure 3a, $\delta_f/l_{diff}$ and $V_t/V_{Iv}$ are plotted as a function of the scaled length of the liquid region, $l_l^*$. The stagnant film thickness $\delta_f$ was back-calculated from Equation 6 using $\Omega_e$ and $V_t$ from the mesoscopic simulations. Note that for the single-grain cases $\delta_f$ tends to infinity. The variation of $\delta_f/l_{diff}$ with $l_l^*$ can be best understood by first focusing on the low grain density data for $\Omega_0 =$ 0.15. At the start of growth, $l_t$ has its lowest value and, therefore, $l_l^*$ is highest ($=5.19$). At the early

stages of growth, i.e. for $l_l^* > 2$, $V_t$ is constant and equal to $V_{Iv}$ which indicates that grains are not interacting yet.

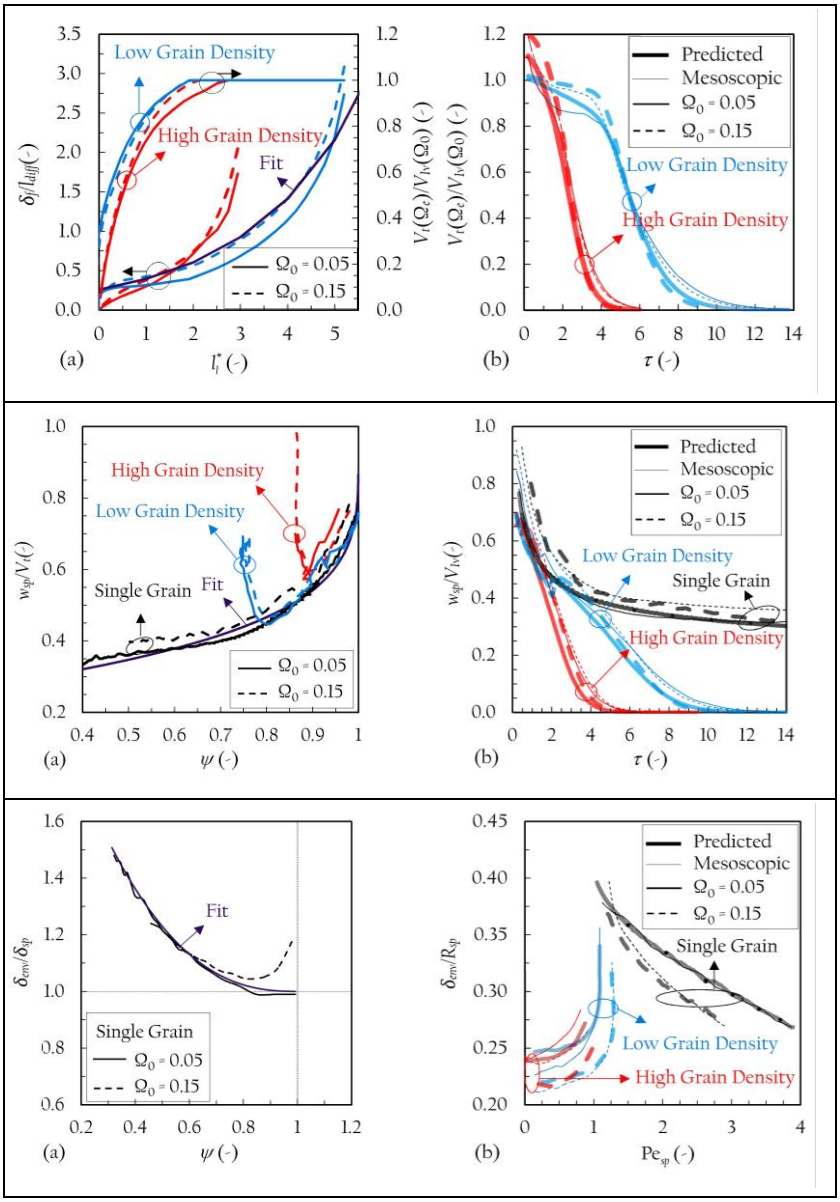


**Figure 3:** (a) Scaled stagnant film thickness $\delta_f/l_{diff}$ (left vertical axis) and normalized dendrite tip velocity $V_t(\Omega_e)/V_{Iv}(\Omega_0)$ (right vertical axis) as a function of the scaled length of the liquid region ahead of the tip up to the symmetry line between two adjacent grains, $l_l^*$; (b) Comparison of predicted and mesoscopic variation of $V_t(\Omega_e)/V_{Iv}(\Omega_0)$ with dimensionless time $\tau = tV_{Iv}^2(\Omega_0)/D_l$.

**Figure 4:** (a) Ratio of the sphere velocity to the tip velocity, $w_{sp}/V_t$, as a function of the envelope sphericity, $\psi$; (b) Comparison of predicted and mesoscopic variation of $w_{sp}/V_{Iv}$ with dimensionless time $\tau = tV_{Iv}^2(\Omega_0)/D_l$.

**Figure 5:** (a) Ratio of the envelope diffusion length to the sphere diffusion length, $\delta_{env}/\delta_{sp}$, as a function of sphericity, $\psi$, for a single grain; (b) Comparison of the predicted and mesoscopic variation of $\delta_{env}/R_{sp}$ with the spherical growth Peclet number, Pe$_{sp}$.

However, due to solute rejection, $\Omega_e$ decreases as soon as growth starts (not shown due to space limitations). A constant $V_t$ along with a decreasing $\Omega_e$ causes $\delta_f$ to decrease relatively rapidly for $l_l^* > 2$. At $l_l^* \approx 2$, $V_t/V_{Iv}$ starts to decrease from unity, which indicates that the grains are starting to interact. For $l_l^* < 2$, $V_t/V_{Iv}$ keeps decreasing; therefore, $l_{diff}$ increases and $\delta_f/l_{diff}$ decreases. It should be mentioned that the decrease in $\delta_f/l_{diff}$ for $l_l^* < 2$, is only due to the increase in $l_{diff}$. During the final stages of growth $V_t \to 0$, $l_{diff} \to \infty$, and $l_l^*$, $\delta_f/l_{diff} \to 0$. Despite the minor spread, which can be expected to be due to the initial transient in the mesoscopic simulations, low-grain-density curves at the two different values of $\Omega_0$ collapse. Next, the low- and high-grain-density curves are compared. The curves for the high grain density case behave in a similar fashion, with the solutal interactions starting again at $l_l^* \approx 2$. All results for $\delta_f/l_{diff}$ are fit a single curve that is given by:

$$\delta_f = \left[0.26\exp\left(0.43 l_l^*\right)\right] l_{diff} \qquad (9)$$

Equation 9, along with Equation 6 and the mesoscopic values of $\Omega_e$, are then used to predict $V_t$. The predictions are compared with the mesoscopic results in Figure 3b where $V_t/V_{Iv}$ is plotted against the dimensionless time $\tau = tV_{Iv}^2/D_l$. The good agreement between the predicted and mesoscopic values of $V_t$ verifies Equation 9.

In Figure 4a, $w_{sp}/V_t$ is plotted as a function of $\psi$. To calculate $w_{sp}$, $R_{sp}$ was first calculated from $R_{sp} = \left[3/(4\pi n)\right]^{1/3} L_{REV} \mathcal{G}_{env}^{1/3}$, where $n$ is the effective number of grains inside the REV (unity for a single grain

and two for multiple grains), $g_{env}$ is the envelope volume fraction, and $L_{REV}$ is the side length of the REV. It can be seen that for the single grain cases, $w_{sp}/V_t$ decreases monotonically as $\psi$ decreases. Since the data for the two different values of $\Omega_0$ collapse, $w_{sp}/V_t$ is indeed a function of $\psi$ only, and the single grain data can be fit to a single curve. Next, the high and low grain density curves are analyzed. These curves fall onto the single grain data only initially for high sphericities. At some critical sphericity (0.8 or 0.9), $w_{sp}/V_t$ for the multigrain cases increases steeply, while the sphericity remains almost constant. This steep increase can be attributed to $V_t$ in the denominator decreasing due to growth interactions. Neglecting this effect, all data for the equivalent sphere growth velocity are fit by the following equation:

$$w_{sp} = \left[1 - 0.76\left(1-\psi\right)^{0.22}\right] V_t \qquad (10)$$

Next, Equations 8–10, along with Equation 6 and the mesoscopic values of $\Omega_c$, are used to predict $w_{sp}$. The predictions are compared with the mesoscopic results in Figure 4b, where $w_{sp}/V_{lv}$ is plotted vs. $\tau$. The good agreement between the predicted and mesoscopic values of $w_{sp}/V_{lv}$ verifies Equation 10.

In Figure 5a, the normalized envelope diffusion length $\delta_{env}/\delta_{sp}^{FG}$ for the single grain cases is plotted as a function of $\psi$. $\delta_{env}$ was back calculated from Equation 2 using mesoscopic values for all the other quantities. It can be seen that as $\psi$ decreases during growth, $\delta_{env}/\delta_{sp}^{FG}$ increases monotonically above unity. Hence, the diffusion length for a complex shaped dendritic envelope is always greater than the diffusion length for the volume-equivalent sphere. Since the data for the two different initial undercoolings collapse, $\delta_{env}/\delta_{sp}^{FG}$ is indeed a function of $\psi$ only. A curve fit to the data for the single grain is given by:

$$\delta_{env} = \left[1 + 1.3 \times \left(1-\psi\right)^{2.5}\right] \delta_{sp} \qquad (11)$$

Note that the superscript "FG" (standing for free growth) in $\delta_{sp}^{FG}$ is dropped because, as shown next, Equation 11 is also valid for multigrain growth. In Figure 5b, predictions of $\delta_{env}$ for all single and multigrain cases are compared with the mesoscopic values of $\delta_{env}$. When calculating $\delta_{env}$ from Equation 11, $\delta_{sp}$ is obtained from the last equality in Equation 4 for the single-grain cases, and from the $\delta_{sp}$ equation in Martorano et al. [3] for the multigrain cases. In all cases, mesoscopic values of $\psi$, $R_{sp}$, and $\mathrm{Pe}_{sp}$ are used as input. The good overall agreement between the predicted and mesoscopic values of $\delta_{env}/R_{sp}$ verifies Equation 11.

## Conclusions

Results from a previously developed mesoscopic envelope model are used to develop constitutive relations for a macroscopic (volume averaged) model of equiaxed growth. Relations are proposed for the envelope sphericity, primary tip and volume-equivalent sphere velocities, and average diffusion length. The relations are verified against the mesoscopic results for a range of initial undercoolings and grain densities, including a single grain. These relations can now be used in macroscopic models of equiaxed solidification to more realistically account for the average growth kinetics of and solute diffusion rates from the grains.

## Acknowledgements

This work was financially supported by NASA (NNX14AD69G) and by the French State through the program "Investment in the future" operated by the National Research Agency (ANR) and referenced by ANR-11 LABX-0008-01 (LabEx DAMAS).

## References

1. C.Y. Wang and C. Beckermann, *Metall. Trans. A*, 1993, **24**:2787.
2. M. Torabi Rad and C. Beckermann, *CFD Modelling and Simulation in Materials Processing 2016*, John Wiley & Sons Inc., NJ, 2016, p. 85.
3. Y. Souhar *et al.*, *Comput. Mater. Sci.*, 2016, **112**:304.
4. M.A. Martorano, et al., Metall. *Mater. Trans. A*, 2003, **34**:1657.

SP17

# Solidification Processing 2017

Proceedings of the
**6th Decennial**
**International Conference on**
**Solidification Processing**

25 - 28 July 2017
Beaumont Estate
Old Windsor, UK

**Edited by Z. Fan**

BCAST

Solidification Processing 2017: Proceedings of the
6th Decennial International Conference on Solidification Processing
edited by Professor Zhongyun Fan.

First published in Great Britain in 2017
by BCAST, Brunel University London.



Typeset and printed in the UK by SS Media, Hertfordshire.

ISBN – 978-1-908549-29-7
6th Decennial International Conference on Solidification Processing
c/o Brunel Centre for Advanced Solidification Technology
Brunel University London
Uxbridge
Middlesex
UB8 3PH, UK
www.brunel.ac.uk/bcast